TU-503
May 1, 1996

Top Mass and Isospin Breaking in Dynamical Symmetry Breaking Scenario

T. Asaka, Y. Shobuda, and Y. Sumino

Department of Physics, Tohoku University
Sendai, 980-77 Japan

Abstract

We consider a scenario where the top-quark mass is generated dynamically, and study the implication of the present experimental values for m_t and the T parameter. We assume technicolor-like scenario for inducing the W mass and an effective four fermi operator for inducing the top-quark mass. We also assume that only this four fermi operator is relevant at low energy. Then we estimate in detail the strength G and the intrinsic mass scale M of the four fermi operator. Unitarity bound is used to quantify the strength of G. We find that $G/4\pi \sim \mathcal{O}(1)$ and that M is of the order of $\Lambda_{TC} \simeq 1 \sim 2$ TeV or less. Namely the four fermi operator cannot be treated as 'point-like' around the electroweak scale. Furthermore we estimate the contribution of the four fermi operator to the T parameter. We find that the QCD correction to the top-quark mass function reduces the contribution to the T parameter by about 40%. By comparing the results with the present experimental bound, we obtain another upper bound on M which is typically in several to 10 TeV region.

1 Introduction

The $SU(2) \times U(1)$ gauge theory for describing the electroweak interactions has been very successful both theoretically and experimentally. However, all the experimental tests have been done for its gauge part and we have little knowledge on the electroweak symmetry breaking mechanism so far. In the light of the naturalness problem, we may suppose that there exists some new physics related to the electroweak symmetry breaking at the energy scale 100 GeV $\sim$ 1 TeV. Dynamical symmetry breaking is one of the attractive candidates for the solution to the naturalness problem. We consider this possibility and study the implication of the present experimental data for the top-quark mass[1] and the T-parameter[2, 3, 4].

In dynamical symmetry breaking scenarios such as technicolor models, an effective four fermi operator

$$\mathcal{L} \;=\; \frac{1}{\Lambda^2}\overline{U_L}U_R\overline{t_R}t_L + h.c. \tag{1}$$

is introduced in order to generate the top-quark mass, where Λ represents the new physics scale (extended technicolor scale) and U denotes a new fermion (techni-fermion) introduced in the symmetry breaking sector. When this fermion forms a pair condensate $\left\langle \overline{U_L}U_R \right\rangle \neq 0$, the top quark acquires its mass

$$m_t \sim \frac{\left\langle \overline{U_L}U_R \right\rangle}{\Lambda^2}. \tag{2}$$

Because the condensate also gives mass to the W boson, one may naively expect that the condensate has a same order of magnitude as the electroweak symmetry breaking scale,

$$\left\langle \overline{U_L}U_R \right\rangle^{1/3} \sim \Lambda_{EW} \sim 1 \text{ TeV}. \tag{3}$$

From the observed value of the top-quark mass $m_t \simeq 175$ GeV[1], this naive argument suggests that $1/\Lambda^2 \sim m_t/\Lambda_{EW}^3$, and that the new physics scale Λ is not too far from Λ_{EW}.

During the last decade, there were many analyses of the dynamical symmetry breaking scenarios in the case of a large top-quark mass $m_t > 100$ GeV. In 1985, Appelquist, et al.[5] studied the ρ parameter (T parameter) in the context of extended technicolor models. They pointed out that naively the mass difference between the techni-U and its iso-partner techni-D is proportional to the top-quark mass, so that this difference would contribute to

the T parameter. Also, they noted that an extra isospin violating operator

$$\frac{1}{\Lambda'^2}\overline{Q_R}\gamma^\mu\sigma^3 Q_R\overline{Q_R}\gamma_\mu\sigma^3 Q_R, \tag{4}$$

where $Q_R = (U_R, D_R)^T$, may give a large contribution to the T parameter since Λ' is considered to approximate Λ. (For $m_t \simeq 175$ GeV, the latter effect would be more significant than the former.) It was suggested in Ref.[6] that the T parameter would be enhanced in the walking technicolor scenario. More detailed analyses on the T parameter were given later in Refs.[7, 8]. Recently the experimental constraint on the T parameter has become more severe, and deviation from the standard model prediction is seen to be very small[4]. Reflecting the present constraint, some dynamical symmetry breaking models have been proposed[9, 10] in which the operator (4) is suppressed at low energy. Ref.[11] studied the constraints from the present T parameter and top mass data, and discussed the top-color assisted technicolor model in this context.

In this paper we assume that at low energy the four fermi operators other than (1) can be neglected. We estimate the strength and the intrinsic mass scale of the particular operator (1) in detail on this assumption. We use unitarity argument to quantify the strength of the operator. Then we estimate the contribution of this operator to the T parameter. We include the QCD correction to the top-quark mass function and study its effect on the T parameter.

In order to incorporate the dynamics of symmetry breaking into our analyses, we solve numerically the Schwinger-Dyson and Bethe-Salpeter equations in the improved-ladder approximation[12]. We follow the formalism developed in Refs.[13, 14, 15]; In these papers, taking $f_\pi = 94$ MeV as an only input parameter for QCD, the quantities Λ_{QCD}, $\left\langle\overline{\Psi}\Psi\right\rangle$, m_ρ, m_{a_1}, m_{a_0}, f_ρ and f_{a_1} have been calculated, which meet the experimental values within 20$\sim$30% accuracy for Λ_{QCD},$\cdots$,m_{a_0} and within a factor of 2 for f_ρ and f_{a_1}. Thus, we expect to study the dynamical effect semi-quantitatively using the formalism.

In Section 2 we present our assumption on the dynamical symmetry breaking scenario. Then we estimate the strength of the four fermi operator from the observed top-quark mass and W boson mass in Section 3. Using the result, the contributions to the T parameter are estimated in Section 4. Conclusion and discussion are given in Section 5.

The explicit formulas of the Schwinger-Dyson and Bethe-Salpeter equations, as well as other equations used in our numerical analyses, are collected in Appendix.

2 Symmetry Breaking Sector and Four Fermi Operator

In this section we explain our assumption on the scenario of dynamical generation of the top-quark mass.

First, we assume technicolor-like scenario[16] for breaking electroweak gauge symmetry. We introduce non-standard-model fermions following the one-doublet technicolor (TC) model as

$$Q_L = \begin{pmatrix} U \\ D \end{pmatrix}_L, \qquad U_R, \qquad D_R. \tag{5}$$

The weak hypercharges are assigned as $Y(Q_L) = 0$, $Y(U_R) = 1/2$, and $Y(D_R) = -1/2$. These fermions belong to the fundamental representation of $SU(N_{TC})$ gauge group, and they form the pair condensates

$$\left\langle \overline{U_L} U_R \right\rangle \neq 0 \qquad \text{and} \qquad \left\langle \overline{D_L} D_R \right\rangle \neq 0 \tag{6}$$

via the $SU(N_{TC})$ gauge interaction. Later when we solve the Schwinger-Dyson equations numerically, we will deal with both the technicolor-like and walking-technicolor-like[17] scenarios by varying the running behavior of the gauge coupling constant. In the following analyses, we consider only the cases $N_{TC} = 2$ and 3 taking into account the present stringent experimental constraint[4] on the S parameter[2].

Secondly, in order to generate the top-quark mass, we introduce an effective four fermi operator

$$\frac{G}{M^2} \left(\overline{Q_L} U_R\right) \left(\overline{t_R} q_L\right) \ + h.c., \tag{7}$$

where q_L denotes the ordinary quark doublet $(t_L, b_L)^T$. G is a dimensionless coupling and M is the intrinsic mass scale of this operator. Because the four fermi operator cannot be a fundamental interaction, there should be some energy scale above which this operator will resolve, and we call this scale M. In other words, it is the scale where higher dimensional operators neglected in Eq.(7) become relevant. We may neglect the higher dimensional operators if all the energy scales involved in our calculation satisfy $E/M \ll 1$. In particular, since we will incorporate the non-perturbative dynamics of the $SU(N_{TC})$ technicolor interaction by solving the Schwinger-Dyson and Bethe-Salpeter equations, the validity of

our effective treatment of the four fermi operator (7) as a contact interaction would be justified if the technicolor scale Λ_{TC} satisfies $\Lambda_{TC} \ll M$.

We assume that we may neglect all effective four fermi operators other than (7) which would be induced at low energy in the models such as extended technicolor models[18]. (See, however, discussion in Section 5.) This is because an operator such as Eq.(4) would give a very large contribution to the T parameter. We do not consider the dynamical origin of the operator (7) in this paper.

3 Strength and Mass Scale of Four Fermi Operator

In this section, we estimate the strength G and the intrinsic mass scale M of the four fermi operator (7) from the observed top-quark and W boson masses.

3.1 Relation between G and M

First, we solve numerically the Schwinger-Dyson equation depicted diagrammatically in Fig.1 for the mass function Σ of techni-U or techni-D fermion[13]. In order to set mass scale in the numerical calculation, we use the charged decay constant $F_{\pi^\pm}$, which is obtained by solving the homogeneous Bethe-Salpeter equation[13] or using the Pagels-Stokar's formula[19]. (Both results are in good agreement.) From the W boson mass M_W, $F_{\pi^\pm}$ is normalized as

$$F_{\pi^\pm} = \frac{2M_W}{g} \simeq 250 \text{ GeV}, \tag{8}$$

where g is the $SU(2)_L$ gauge coupling constant.

As shown in Fig.2, the top quark acquires its mass m_t through the four fermi operator (7), and m_t can be calculated as

$$m_t = \frac{G}{M^2} \left\langle \overline{U_L} U_R \right\rangle_M , \tag{9}$$

where

$$\begin{aligned} \left\langle \overline{U_L} U_R \right\rangle_M &= \frac{1}{2} \int_{p_E^2 \le M^2} \frac{d^4p}{(2\pi)^4} \mathrm{tr} \left(\frac{i}{\not{p} - \Sigma(p)} \right) \\ &= \frac{N_{TC}}{8\pi^2} \int_0^{M^2} dx \frac{x\Sigma(x)}{x + \Sigma(x)^2}, \end{aligned} \tag{10}$$

with $x = p_E^2 = -p^2$. Note that we define the intrinsic mass scale M of the four fermi operator (7) as the momentum cut-off of the integral in Eq.(10) since the four fermi operator will resolve above the energy scale M.

By calculating the condensate $\left\langle \overline{U_L} U_R \right\rangle_M$ for a given M, and substituting the top-quark mass $m_t \simeq 175$ GeV[1] in Eq.(9), we obtain the coupling G as a function of M. We show the G-M relation in Figs.3 for the $SU(2)$ and $SU(3)$ technicolor cases, and also for the walking technicolor case.* We neglect the region $M \lesssim \Lambda_{TC}$ where our effective treatment of the four fermi operator (7) as a contact interaction breaks down. We define Λ_{TC} as the scale where the leading-logarithmic running coupling constant of technicolor diverges. The values of Λ_{TC} in our numerical estimates are $\Lambda_{TC} \simeq 1.7$, 1.3, and 0.6 TeV for the $SU(2)$, $SU(3)$ technicolor, and the walking technicolor cases, respectively. For the technicolor cases, $G(M)$ is almost proportional to M^2 as M increases, while it is almost proportional to M for the walking technicolor case. These tendencies are consistent with the asymptotic behaviour of the mass function of techni-U[20, 21]:

$$\Sigma(x) \sim \frac{1}{x} (\log x)^{\frac{3C_2}{\beta_0}-1}, \tag{11}$$

where β_0 is the 1-loop β function of the technicolor interaction and $C_2 = (N_{TC}^2 - 1)/2N_{TC}$. It should be noted that for both technicolor and walking technicolor cases, the coupling G should be rather strong, typically $G/4\pi \sim \mathcal{O}(1)$ in order to explain the observed top-quark mass.

3.2 Unitarity Constraint for the Coupling G

We have seen that the coupling G should be quite large. As a criterion for testing the strength of G, we study tree-level unitarity limit related to the four fermi operator (7). There are a few scattering amplitudes induced by this operator at tree-level which increase in high energy and at some energy would violate the unitarity bound. The tree-level unitarity violation occurs at lower energy for larger value of G in general. However, the energy to reach the unitarity limit should be above the scale M, since we have assumed that the four fermi operator (7) can be treated as a contact interaction below the scale M,

* In our analyses, the walking technicolor case corresponds to the $SU(3)$ technicolor theory with one technifermion doublet which is introduced in (5) and ten technifermion singlets under $SU(2)_L \times U(1)_Y$. The 1-loop β-function reduces to approximately 1/3 of the $SU(3)$ technicolor case.

that is, the higher dimensional operators are irrelevant at energy scale $E \ll M$. We see that this requirement leads to the upper bound for G.

Let us consider the two-body to two-body scatterings of fermions via the operator (7) at the energy scale where $E \gg \Lambda_{TC}$. In this energy region the confinement effect of technicolor may be ignored. The tree-level matrix elements of these processes increase quadratically with the center of mass energy. We find that the scattering amplitude for $t\bar{t} \to U\overline{U}$ in $J = 0$ channel will reach the unitarity limit most quickly. The partial-wave amplitude is given by

$$T^{J=0}\left(\sqrt{s}\right) = \frac{\sqrt{N_C N_{TC}}}{8\pi} \frac{G}{M^2}\ s, \tag{12}$$

where $\sqrt{s}$ is the center of mass energy.† We set $m_t = m_U = 0$ considering $E \gg \Lambda_{TC}$. Unitarity limit[23] for an inelastic scattering channel is given by $\left|T^J\right| \leq 1$. We may demand that the tree-level unitarity should not be violated below $\sqrt{s} = M$, that is,

$$\left|T^{J=0}(\sqrt{s} = M)\right| \leq 1, \tag{13}$$

which can be translated to the upper bound for G as

$$G \leq \frac{8\pi}{\sqrt{N_C N_{TC}}}. \tag{14}$$

The bound is so stringent that there are hardly allowed regions in the G-M planes in Figs. 3 for $M > \Lambda_{TC}$. This result suggests that our effective treatment of the four fermi operator as a contact interaction breaks down. Since the coupling G exceeds the perturbative unitarity limit for $M > \Lambda_{TC}$, the higher order corrections of G are large and should modify the tree level amplitude to restore unitrairy at energy scale $E \sim \Lambda_{TC}$. Such corrections induce the higher dimensional operators which become relevant at energy scale $E \sim \Lambda_{TC}$. Thus the scale M above which the operator (7) will resolve is found to be around Λ_{TC} or less.

3.3 Coupled Schwinger-Dyson Equations

From the above discussion, the coupling G should be strong and the non-perturbative effect of the four fermi operator (7) would be significant. Meanwhile, in Subsection 3.1, we only

† In our previous paper[22], we incorrectly omitted the color and technicolor factors in Eq.(12) which come from the normalization of the initial and final states.

considered the $\mathcal{O}(G)$ contribution in estimating the top-quark mass. Here we include part of the non-perturbative effect of the four fermi operator and re-estimate the G-M relation.

For this purpose, we solve the coupled Schwinger-Dyson equations for techni-U and top quark shown diagramatically in Fig.4. Note that the operator (7) affects the mass function of techni-U but not that of techni-D. We re-estimate the coupling $G(M)$, and the results are shown in Figs.5. $G(M)$ is found to decrease compared to the previous analysis. This can be understood by noting that the top-quark loop diagram in Fig.4 gives additive contribution to $\left\langle \overline{U_L} U_R \right\rangle_M$ so that a weaker coupling G is necessary to generate the top-quark mass. The deviations from the previous analyses increase for larger M since the coupling G is larger in this region and the non-perturbative effect is more significant.

3.4 QCD correction

Finally we incorporate QCD correction in estimating the G-M relation. In the previous analyses, we neglected QCD running effect of the top-quark mass function Σ_t. From the renormalization group equation analysis, Σ_t receives QCD correction from m_t to M scale as

$$\Sigma_t(M^2) = \Sigma_t({m_t}^2) \left[\frac{\log({m_t}^2/\Lambda_{QCD}^2)}{\log(M^2/\Lambda_{QCD}^2)} \right]^{\frac{4}{\beta}}, \tag{15}$$

where $\beta = 11 - \frac{2}{3} n_f$ is the lowest order coefficient of the β-function of renormalization group equation of QCD.

We include this running effect by solving the coupled Schwinger-Dyson equations which are shown in Fig.6. (See Appendix for detail.) Again, the coupling $G(M)$ is obtained. The results are given in Figs.7. We find that the coupling becomes smaller in each case. This is because for $\mu > m_t$ the top-quark mass becomes smaller, $\Sigma_t(\mu^2) < m_t$, due to the QCD correction Eq.(15). Nevertheless there are still no allowed regions in the G-M planes for $M > \Lambda_{TC}$.

4 Contributions to T parameter

Because the four fermi operator (7) violates isospin symmetry, one may expect that the results obtained in the previous section may lead to large isospin violating effects. In this section we estimate the contributions of the four fermi operator to the T parameter.

4.1 Contribution of $\Sigma_U - \Sigma_D$

Here we consider the isospin violating effect originating from the difference of techni-U and techni-D mass functions. The contribution of the four fermi operator to the techni-U mass function in the Schwinger-Dyson equations causes this difference. (See Fig.4.) We estimate the T parameter and compare with the present experimental bound, from which we extract another bound for the mass scale M of the four fermi operator.

We calculate the charged and neutral decay constants $F_{\pi^\pm}$ and F_{π^0} from the mass functions of techni-U and D using the generalized Pagels-Stokar's formula[24]. Then the contribution to the T parameter (T_{NEW}) is calculated as

$$\alpha T_{NEW} = \frac{F_{\pi^\pm}^2 - F_{\pi^0}^2}{F_{\pi^0}^2}, \tag{16}$$

where $\alpha = 1/128$ is the fine structure constant. Thus, we can calculate T_{NEW} as a function of G and M.

Let us first consider the case discussed in Subsection 3.3, that is, we neglect the QCD effect on Σ_t. The results are shown in Figs.8 when the coupling G is on the corresponding lines $G = G(M)$ in Fig.5. One sees that T_{NEW} increases with M (or G). This behavior is consistent with the naive estimate of T parameter by the fermion 1-loop calculation[2]

$$T \simeq \frac{N_{TC}}{12\pi \sin^2\theta_W \cos^2\theta_W} \left[\frac{(\Delta m)^2}{M_Z^2}\right], \tag{17}$$

combined with a naive estimate of the mass difference of techni-U and D from the coupled Schwinger-Dyson equations (i.e. the additional term in Fig.4)

$$\Delta m \simeq \frac{N_C}{8\pi^2} G(M)\, m_t. \tag{18}$$

Also we see that T_{NEW} is larger for the walking technicolor case than that of technicolor case for the same M. This tendency has been pointed out by Chivukula[6].

Comparing the results with the present experimental data on the T parameter[4]

$$T_{exp} - T_{SM}(m_t = 175 \text{ GeV}, m_H = 1 \text{ TeV}) = 0.32 \pm 0.20, \tag{19}$$

we may put 3σ upper bounds for the intrinsic mass scale M as follows:

$$\begin{aligned} M &\lesssim 7 \text{ TeV} && \text{for } SU(2) \text{ technicolor} \\ M &\lesssim 5 \text{ TeV} && \text{for } SU(3) \text{ technicolor} \\ M &\lesssim 4 \text{ TeV} && \text{for walking technicolor} \end{aligned} \tag{20}$$

Note that the bound is more stringent for the walking technicolor case.

Next, we inculde the QCD correction on Σ_t. The results are also shown in Figs.8. Note that the QCD correction reduces T_{NEW} by about 40%. This can be understood from Eqs.(17) and (18) if we note that both $G(M)$ and $\Sigma_t(\mu^2)$ ($\mu > m_t$) get smaller by the QCD correction. (See Subsection 3.4.) Similarly, 3σ upper bounds for M are obtained:

$$\begin{aligned} M &\lesssim 12 \text{ TeV} \qquad && \text{for } SU(2) \text{ technicolor} \\ M &\lesssim 9 \text{ TeV} \qquad && \text{for } SU(3) \text{ technicolor} \\ M &\lesssim 4 \text{ TeV} \qquad && \text{for walking technicolor} \end{aligned} \tag{21}$$

4.2 Contribution of $\overline{U_R}\gamma_\mu U_R \overline{U_R}\gamma^\mu U_R$

We started our analyses assuming that only the four fermi operator (7) exists at low energy in order to dispense with the potentially dangerous operator

$$C\,\overline{U_R}\gamma_\mu U_R \overline{U_R}\gamma^\mu U_R, \tag{22}$$

which would induce a large T parameter[5]. We found in the previous section, however, that the higher order corrections of the operator (7) cannot be neglected. In fact, the above operator (22) is generated by four insertions of the operator (7) at three-loop level. (Fig.9) From a dimensional analysis of this graph, we estimate

$$C \;\sim\; -\frac{N_C^2}{(4\pi)^6}\frac{G^4}{M^2}. \tag{23}$$

Then the contribution of the operator (22) to the T parameter can be estimated as

$$T \sim 6\times 10^{-2}\,\frac{N_{TC}(N_{TC}+1)}{12}\left(\frac{m_U}{1\,\text{TeV}}\right)^4\left(\frac{2\,\text{TeV}}{M}\right)^2\left(\frac{G}{4\pi}\right)^4\left(\log\frac{\Lambda_{TC}^2}{m_U^2}\right)^2. \tag{24}$$

We should note that the three-loop graph is very sensitive to the cut-off of the loop momenta. Therefore the estimated value Eq.(24) may change by a factor ~ 10 by a slight change of the cut-off and therefore it may give a non-negligible contribution to the T parameter. We should also remark that Eq.(23) may suggest self-inconsistency of our assumption that we neglect all four fermi operators other than (7). We will discuss this point in the next section.

5 Conclusion and Discussion

In this paper, within a scenario where the top-quark mass is generated dynamically, we estimated the coupling G and the intrinsic mass scale M of the four fermi operator that induces the top-quark mass. Also, we studied the contribution of this four fermi operator to the T parameter.

Throughout our analyses, we made the following assumptions:

- The W and Z bosons acquire their masses in the one-doublet technicolor-like scenario.
- The top quark acquires its mass via the effective four fermi operator (7). We consider only this four fermi operator and neglect all other effective four fermi operators that may be induced in various dynamical models.

We incorporated the dynamics of $SU(N_{TC})$ gauge interaction by solving the Schwinger-Dyson and Bethe-Salpeter equations numerically in the improved-ladder approximation (in all the analyses except in Subsection 4.2).

In Section 3, we studied in detail the strength G and the intrinsic mass scale M of the four fermi operator using M_W and m_t as the input parameters. We obtained G as a function of M in the region $M > \Lambda_{TC}$, and found that G is rather strong, $G/4\pi \sim O(1)$. Then we compared the coupling G with that demanded by the tree-level unitarity bound. Our results suggest that M should be of the order of $\Lambda_{TC} \simeq 1 \sim 2$ TeV or less, so that the four fermi operator cannot be treated as 'point-like' at scale $E \sim \Lambda_{TC}$. Conventionally the four fermi operator (7) has been treated perturbatively in many papers, but the unitarity saturation shows that such a treatment is inconsistent with the presently observed top-quark mass. We included part of the higher order corrections of the four fermi operator (7) by solving the coupled Schwinger-Dyson equations. Also we included the effect of QCD correction on the top-quark mass function. These effects, respectively, are found to reduce $G(M)$.

In Section 4 we studied the contributions of the four fermi operator (7) to the T parameter. First we estimated the contribution of the difference between the mass functions of techni-U and techni-D. We found that the QCD correction is large and reduces the contribution to the T parameter by about 40%. The estimated T parameter is within the present experimental bound. Then we used the experimental bound to obtain another upper bound for M, and found that typically M is less than 10 TeV. The bound on M

is more stringent for the walking technicolor case. Secondly we pointed out that the dangerous operator $\overline{U_R}\gamma_\mu U_R\overline{U_R}\gamma^\mu U_R$ would be generated by the four fermi operator (7) at the three-loop level, and estimated its contribution to the T parameter from a dimensional analysis. The contribution may become non-neglegible.

We found that the four fermi operator (7) cannot be treated as 'point-like' at scale $E \sim \Lambda_{TC}$. In order to make a more consistent analysis, one needs to specify the 'structure' of the four fermi operator, i.e. specify the dynamical origin of this operator. One way is to rewrite the four fermi operator in terms of a massive-gauge-boson exchange interaction as in the extended technicolor models. We are currently making further analyses in this direction.

We started our analyses on the assumption that all four fermi operators except Eq.(7) can be neglected. We found, however, that other four fermi operators generated in higher orders of the operator (7) may be non-negligible. (e.g. The operator $\overline{U_R}\gamma_\mu U_R\overline{U_R}\gamma^\mu U_R$.) This self-inconsistency seems to put certain constraints when constructing a viable model of dynamical electroweak symmetry breaking. Namely, suppose one could construct an extended technicolor model that has ETC gauge bosons which induce only the four fermi operator (7) at tree level. Then other four fermi operators induced at higher loops would be suppressed by powers of Λ_{TC}/M, but this factor is close to one for the top-quark mass $\simeq 175$ GeV.

Acknowledgments

We are grateful to K. Fujii, K. Hagiwara, K. Hikasa, J. Hisano, B. Holdom, N. Maekawa, T. Moroi, H. Murayama, M. Peskin, and J. Terning for fruitful discussion.

Appendix

In this appendix, we list the Schwinger-Dyson equations as well as other formulas which are used in our numerical analyses.

In Section 3, we solved the coupled and non-coupled Schwinger-Dyson equations in the improved ladder approximation for the mass functions of techni-U, techni-D and top quark (Σ_U, Σ_D and Σ_t). All these equations can be written in the following forms:

$$\begin{aligned}
\Sigma_U(x) &= \frac{\lambda(x)}{4x}\int_0^x dy \frac{y\Sigma_U(y)}{y+\Sigma_U^2(y)} + \int_x^{\Lambda^2} dy \frac{\lambda(y)\Sigma_U(y)}{4\left(y+\Sigma_U^2(y)\right)} \\
&\quad + A_1 \cdot \frac{N_C}{8\pi^2}\frac{G}{M^2}\int_0^{M^2} dy \frac{y\Sigma_t(y)}{y+\Sigma_t^2(y)}, \\
\Sigma_D(x) &= \frac{\lambda(x)}{4x}\int_0^x dy \frac{y\Sigma_D(y)}{y+\Sigma_D^2(y)} + \int_x^{\Lambda^2} dy \frac{\lambda(y)\Sigma_D(y)}{4\left(y+\Sigma_D^2(y)\right)}, \\
\Sigma_t(x) &= \frac{N_{TC}}{8\pi^2}\frac{G}{M^2}\int_0^{M^2} dy \frac{y\Sigma_U(y)}{y+\Sigma_U^2(y)} \\
&\quad + A_2\left[\frac{\lambda_{QCD}(x)}{4x}\int_0^x dy \frac{y\Sigma_t(y)}{y+\Sigma_t^2(y)} + \int_x^{\Lambda^2} dy \frac{\lambda_{QCD}(y)\Sigma_t(y)}{4(y+\Sigma_t^2(y))}\right],
\end{aligned} \tag{25}$$

where $\lambda(x)$ and $\lambda_{QCD}(x)$ denote the running coupling constants for technicolor and color interactions, respectively.

According to Ref.[13], we take $\lambda(x)$ as follows:

$$\lambda(x) \;=\; \lambda_0 \times \begin{cases} C & \text{if } t \le t_0 \\ C - \dfrac{1}{2}\dfrac{A}{(1+At_{IF})^2}\dfrac{(t-t_0)^2}{(t_{IF}-t_0)} & \text{if } t_0 \le t \le t_{IF} \\ \dfrac{1}{1+At} & \text{if } t_{IF} \le t \end{cases} \tag{26}$$

with

$$t = \ln x \quad \text{and} \quad C = \frac{1}{2}\frac{A(t_{IF}-t_0)}{(1+At_{IF})^2} + \frac{1}{1+At_{IF}},$$

where $\lambda_0/A = 12C_2/\beta_0$ and β_0 is the 1-loop order coefficient of the β-function and $C_2 = (N_{TC}^2-1)/2N_{TC}$ represents the second Casimir. Thus, above the infrared cut-off scale $t \ge t_{IF}$, $\lambda(x)$ is related to the 1-loop running coupling constant $g_{TC}(x)$ as

$$\lambda(x) \;=\; \frac{3}{4\pi^2}\, C_2\, g_{TC}^2(x). \tag{27}$$

In our numerical calculation, we fix the point $t_0 = \ln \mu_0^2$ relative to Λ_{TC} and consider the infrared cut-off scale t_{IF} as a free parameter. We define Λ_{TC} as the point where the leading logarthmic running coupling constant diverges:

$$1 + A \ln \Lambda_{TC}^2 = 0. \tag{28}$$

As for all the dimensionful quantities in our calculation, we set scale by normalizing the decay constant as in Eq.(8).

For the QCD coupling constant, $\lambda_{QCD}(x)$ takes the same form as Eq.(26). Above the infrared cut-off scale of QCD, $\lambda_{QCD}(x)$ can be expressed by the 1-loop running coupling constant $g_{QCD}(x)$ as

$$\lambda(x) \;\; = \;\; \frac{3}{4\pi^2}\, C_2^{QCD}\; g_{QCD}^2(x). \tag{29}$$

where $C_2^{QCD} = (N_C^2 - 1)/2N_C$ and $N_C = 3$. We set the mass scale of QCD by taking Λ_{QCD} = 200 MeV.

1. In Subsection 3.1, we solved the equation (25) for the techni-U setting

$$A_1 = 0, \quad \text{and} \quad \Lambda = \infty, \tag{30}$$

   which is given diagrammatically in Fig.1.

2. In Subsection 3.3, we solved the coupled Schwinger-Dyson equations (Fig.4), which correspond to

$$A_1 = 1, \quad A_2 = 0, \quad \text{and} \quad \Lambda = M. \tag{31}$$

3. In Subsection 3.4, we solved the coupled Schwinger-Dyson equations including the QCD correction (Fig.6), which correspond to

$$A_1 = 1, \quad A_2 = 1, \quad \text{and} \quad \Lambda = M. \tag{32}$$

For the above coupled Schwinger-Dyson equations (31) and (32), we take the ultraviolet cutoff scale[25] as $\Lambda = M$.

As mentioned earlier, we calculated the charged decay constant $F_{\pi^\pm}$ in order to set the mass scale. We define the decay constant as,

$$\langle 0 |\, \bar{Q}_L \gamma^\mu T^b Q_L(0)\, | \pi^a(q) \rangle = \frac{i}{2} F_\pi^{ab} q^\mu, \tag{33}$$

where T^a (a=1,2,3) is the generator of $SU(2)_L$. Then the charged and neutral decay constants, respectively, are given by $F_{\pi^\pm} \equiv F_\pi^{11} = F_\pi^{22}$ and $F_{\pi^0} \equiv F_\pi^{33}$.

For the isospin symmetric case ($F_{\pi^0} = F_{\pi^\pm} = F_\pi$), we obtained F_π by solving the homogeneous Bethe-Salpeter (BS) equation[13], or using the Pagels-Stokar's formula[19].

According to Ref.[13], the BS amplitude χ for the $J^{PC} = 0^{-+}$ massless state (the techni-pion state) is defined by

$$\begin{aligned}\int d^4r\ e^{ipr} \langle 0|\, T\ \Psi_\alpha^{f,i}(x+r/2)\overline{\Psi}_\beta^{f',j}(x-r/2)\,|\pi^a(q)\rangle \\ = \frac{1}{\mathcal{N}}\ \delta_{ij}\ T^a_{ff'}\ e^{-iqx}\ \chi_{\alpha\beta}(p,q)\end{aligned} \tag{34}$$

where $i, j, \cdots$ denote the technicolor indices, $f, f', \cdots$ the flavor indices, and $\alpha, \beta, \cdots$ the spinor indices, and Ψ denotes the techni-fermion. $\mathcal{N}$ is introduced as the normalization for the amplitude. From the spinor structure and the quantum number $J^{PC} = 0^{-+}$, the bispinor part $\chi_{\alpha\beta}$ is expanded into following invariant amplitudes:

$$\chi(p,q) = \left[S(p;q) + P(p;q)(p\cdot q)\ \not{p} + Q(p;q)\ \not{q} + \frac{1}{2}T(p;q)\,(\not{p}\,\not{q} - \not{q}\,\not{p})\right]\gamma_5. \tag{35}$$

Here the above amplitudes are found to be even functions of $(p\cdot q)$ from the charge conjugation property. Using the on-shell condition of π ($q^2 = 0$), each amplitude can be expanded as

$$\begin{aligned} S(p,q) &= S_0(p^2) + \sum_{I=1}^{\infty}(p\cdot q)^{2I} S_I(p^2), \\ P(p,q) &= P_0(p^2) + \sum_{I=1}^{\infty}(p\cdot q)^{2I} P_I(p^2), \quad \text{etc.} \end{aligned} \tag{36}$$

Then we can write down the decay constant F_π in terms of coefficients of above expansion. The definition of F_π leads

$$F_\pi i q_\mu = -\frac{1}{2\mathcal{N}}\int \frac{d^4p}{(2\pi)^4}\ \mathrm{tr}\left[\gamma_\mu\gamma_5\chi_{\alpha\beta}(p,q)\right], \tag{37}$$

and after angular integration, it takes the form

$$F_\pi^2 = \frac{N_{TC}}{16\pi^2}\int_0^\infty dx x\left[4Q_0(x) - xP_0(x)\right], \tag{38}$$

where $x = p_E^2$ and we choose $\mathcal{N} = F_\pi/2$. Thus we only need the first terms in the expansion Eq.(36) to calculate the decay constant.

In order to calculate $P_0(x)$ and $Q_0(x)$, we solve the homogeneous Bethe-Salpeter equation for χ in the improved ladder approximation, as shown in Fig.10 diagrammatically, as follows:

$$\begin{aligned}
& [\not{p}+ \not{q}/2 - \Sigma(p+q/2)]\ \chi(p,q)\ [\not{p}- \not{q}/2 - \Sigma(p-q/2)] \\
= \ & i\int \frac{d^4k}{(4\pi)^4}\frac{4\pi^3}{3}\lambda\left(max(p_E^2,k_E^2)\right) \\
& \times\gamma^\mu\ \chi(k,q)\ \gamma^\nu\ \frac{1}{(p-k)^2}\left[g_{\mu\nu}-\frac{(p-k)_\mu(p-k)_\nu}{(p-k)^2}\right], \qquad (39)
\end{aligned}$$

where we use λ defined in Eq.(26). We expand this BS equation in power of $(p\cdot q)$ and solve it to first order in $(p\cdot q)$ because $Q_0(x)$ and $P_0(x)$ are first order terms in q. Explicit forms of this integral equations are found in Ref.[13]. By using the numerical solutions for them, we can calculate F_π using the formula (38).

We also use the Pagels-Stokar's formula[19] to obtain F_π:

$$F_\pi^2 = \frac{N_{TC}}{4\pi^2}\int_0^\infty dx\ \frac{x}{4}\ \frac{4\Sigma^2 - x\frac{d}{dx}\Sigma^2}{(x+\Sigma^2)^2}. \qquad (40)$$

Both F_π's obtained from the homogeneous Bethe-Salpeter equation and from the Pagels-Stokar's formula are in good agreement.

On the other hand, for the case where the isospin symmetry is broken, we calculate the charged decay constant $F_{\pi^\pm}$ and the neutral one F_{π^0} using the generalized Pagels-Stokar's formulas[24]:

$$F_{\pi^0}^2 = \frac{N_{TC}}{8\pi^2}\int_0^\infty dx\ I_0(\Sigma_U,\Sigma_D), \qquad (41)$$

$$F_{\pi^\pm}^2 = \frac{N_{TC}}{8\pi^2}\int_0^\infty dx\ I_\pm(\Sigma_U,\Sigma_D), \qquad (42)$$

with

$$I_0(\Sigma_U,\Sigma_D) \equiv x\ \frac{\Sigma_U^2 - \frac{x}{4}\ \frac{d}{dx}\Sigma_U^2}{(x+\Sigma_U^2)^2} + x\ \frac{\Sigma_D^2 - \frac{x}{4}\ \frac{d}{dx}\Sigma_D^2}{(x+\Sigma_D^2)^2}, \qquad (43)$$

$$\begin{aligned}
I_\pm(\Sigma_U,\Sigma_D) \equiv\ & x\ \frac{\Sigma_U^2+\Sigma_D^2 - \frac{x}{4}\ \frac{d}{dx}(\Sigma_U^2+\Sigma_D^2)}{(x+\Sigma_U^2)(x+\Sigma_D^2)} \\
+\ & \frac{x^2}{2}\ \frac{\Sigma_U^2-\Sigma_D^2}{(x+\Sigma_U^2)(x+\Sigma_D^2)}\ \frac{d}{dx}\log\left[\frac{x+\Sigma_U^2}{x+\Sigma_D^2}\right]. \qquad (44)
\end{aligned}$$

In our calculation, we cut off the integral at M instead of infinity in Eqs.(41) and (42). The approximation would be valid since $\Sigma_U(x)$ and $\Sigma_D(x)$ vanishes swiftly the region $x \gg \Lambda_{TC}^2$.

References

[1] F. Abe, *et al.* (CDF Collaboration), *Phys. Rev. Lett.* **74** (1995) 2626;
S. Abachi, *et al.* (D0 Collaboration), *Phys. Rev. Lett.* **74** (1995) 2632.

[2] M. Peskin and T. Takeuchi, *Phys. Rev. Lett.* **65** (1990) 964; *Phys. Rev.* **D46** (1992) 381.

[3] C. Burgess, S. Godfrey, H. König, D. London, and I. Maksymyk, *Phys. Rev.* **D49** (1994) 6115;
K. Hagiwara, D. Haidt, C.S. Kim, S. Matsumoto, *Z. Phys.* **C64** (1994) 559.

[4] S. Matsumoto, *Mod. Phys. Lett.* **A10** (1995) 2553.

[5] T. Appelquist, M.J. Bowick, E. Cohler and A.I. Hauser, *Phys. Rev. Lett.* **53** (1984) 1523; *Phys. Rev.* **D31** (1985) 1676.

[6] R. Chivukula, *Phys. Rev. Lett.* **61** (1988) 2657.

[7] T. Appelquist, T. Takeuchi, M.B. Einhorn and L.C.R. Wijewardhana, *Phys. Lett.* **B232** (1989) 211.

[8] M.B. Einhorn and D.Nash, *Nucl. Phys.* **B371** (1992) 32.

[9] B. Holdom, *Phys. Lett.* **B336** (1994) 85; (hep-ph/9510249).

[10] T. Asaka, in preparation.

[11] R. Chivukula, B. Dobrescu, and J. Terning, (hep-ph/9506450).

[12] V.A. Miransky, *Sov. J. Nucl. Phys.* **38** (1984) 280;
K. Higashijima, *Phys. Rev.* **D29** (1984) 1228.

[13] K.-I. Aoki, M. Bando, K. Hasebe, T.Kugo and H. Nakatani, *Prog. Theor. Phys.* **82** (1989) 1151;
K.-I. Aoki, M. Bando, T. Kugo, M.G. Mitchard and H. Nakatani, *Prog. Theor. Phys.* **84** (1990) 683.

[14] K.-I. Aoki, T. Kugo and M.G. Mitchard, *Phys. Lett.* **266B** (1991) 467.

[15] M. Bando, M. Harada, and T. Kugo, *Prog. Theor. Phys.* **91** (1994) 927.

[16] S. Weinberg, *Phys. Rev.* **D13** (1976) 947; *Phys. Rev.* **D19** (1979) 1277;
L. Susskind, *Phys. Rev.* **D20** (1979) 2619;
For review, see E.Farhi and L. Susskind, *Phys. Rep.* **74** (1981) 277.

[17] B. Holdom, *Phys. Lett.* **150B** (1985) 301;
K. Yamawaki, M. Bando and K. Matumoto, *Phys. Rev. Lett.* **56** (1986) 1335;
T. Akiba and T. Yanagida, *Phys. Lett.* **169B** (1986) 432;
T. Appelquist, D. Karabali and L.C.R. Wijewardhana, *Phys. Rev. Lett.* **57** (1986) 957.

[18] S. Dimopoulos and L. Susskind, *Nucl. Phys.* **B155** (1979) 237;
E. Eichten and K. Lane, *Phys. Lett.* **90B** (1980) 125.

[19] H. Pagels and S. Stokar, *Phys. Rev.* **D20** (1979) 2947.

[20] H.D. Politzer, *Nucl. Phys.* **B117** (1976) 397.

[21] K-I. Aoki, M.Bando, T. Kugo and M.G. Mitchard, *Prog. Theor. Phys.* **85** (1991) 355.

[22] T. Asaka, N. Maekawa, T. Moroi, Y. Shobuda, and Y. Sumino, Tohoku University preprint TU-483 (hep-ph/9505371).

[23] See, for example, C. Itzykson and J. Zuber, "Quantum Field Theory" (McGraw-Hill, 1980).

[24] V.A. Miransky, M. Tanabashi and K. Yamawaki, *Phys. Lett.* **221B** (1989) 177; *Mod. Phys. Lett.* **A4** (1989) 1043.

[25] More precisely in these equations we should set, respectively,

$$A_2 = 0, \quad \Lambda = \infty, \quad \text{and} \quad \begin{cases} A_1 = 1 & \text{for} \quad x \leq M^2 \\ A_1 = 0 & \text{for} \quad x \geq M^2, \end{cases}$$

and

$$A_2 = 1, \quad \Lambda = \infty, \quad \text{and} \quad \begin{cases} A_1 = 1 & \text{for} \quad x \leq M^2 \\ A_1 = 0 & \text{for} \quad x \geq M^2. \end{cases}$$

Here, note that the four fermi operator (7) resolves (and is crudely set equal to zero) above the scale M. The mass functions of techni-fermions ($\Sigma_U(x)$ and $\Sigma_D(x)$) and also

the running coupling constant $\lambda(x)$, however, decrease in the energy region $x \gg \Lambda_{TC}^2$, and we may replace the ultraviolet cut-off Λ by M approximately. Thus we have only to know the mass fuctions below the scale M and solve the coupled equations Eqs.(31) and (32). In fact, we see in Figs.5 that the obtained results from the coupled Schwinger-Dyson equations Eq.(31) are close to those from the Schwinger-Dyson equation Eq.(30) as the mass scale M approaches Λ_{TC}. Thus we consider this approximation does not change our results.

Figure Captions

Figure 1: The graphical representation for the Schwinger-Dyson equation for the mass function of techni-U (or techni-D) in the improved ladder approximation. The blob denotes the mass function for techni-U.

Figure 2: The diagram for the top-quark mass. The line with a blob denotes the full propagator for techni-U.

Figure 3: The allowed regions in the G-M plane for (A) $SU(N_{TC})$ technicolor cases and for (B) walking technicolor case. Curved lines represent the coupling $G(M)$ obtained from Eq.(9). The curves are drawn only in the region $M > \Lambda_{TC}$. Horizontal lines show the upper bounds for G obtained from the unitarity limit. For $SU(N_{TC})$ technicolor cases, the solid and dot-dashed lines correspond to $N_{TC} = 2$ and $N_{TC} = 3$, respectively.

Figure 4: The graphical representation for the coupled Schwinger-Dyson equations for the mass functions of techni-U and top quark.

Figure 5: The allowed regions in the G-M plane obtained by solving the coupled Schwinger-Dyson equations. The notations are same as Fig.3. Previous results (Fig.3) are also shown in dots for comparison.

Figure 6: The graphical representation for the coupled Schwinger-Dyson equations for the mass functions of techni-U and top quark including the QCD correction to the top quark.

Figure 7: The allowed regions in the G-M plane obtained by solving the coupled Schwinger-Dyson equations including the QCD correction. The notations are same as Fig.3. Previous results (Figs.3 and 5) are also shown in dots for comparison.

Figure 8: The contribution to the T parameter, T_{NEW}, from $\Sigma_U - \Sigma_D$ when the coupling is on the curved lines $G = G(M)$ in Figs.5 and 7, for (A) $SU(2)$ technicolor, (B) $SU(3)$ technicolor, and (C) walking technicolor case. The dotted lines are T_{NEW} without QCD correction and the solid lines are the ones including the QCD correction.

Figure 9: A three-loop Feynman diagram that induces the operator $\overline{U}_R\gamma^\mu U_R\overline{U}_R\gamma_\mu U_R$.

Figure 10: The graphical representation for the homogeneous Bethe-Salpeter equation for the BS amplitude χ.

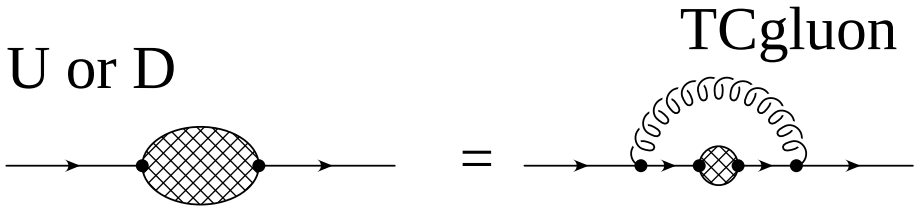

Fig. 1

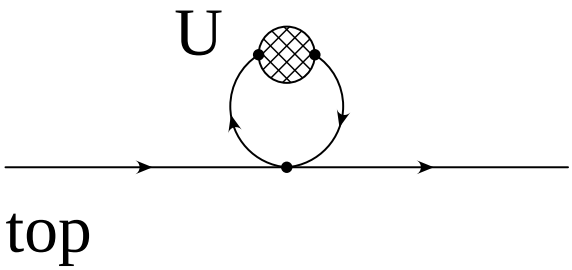

Fig. 2

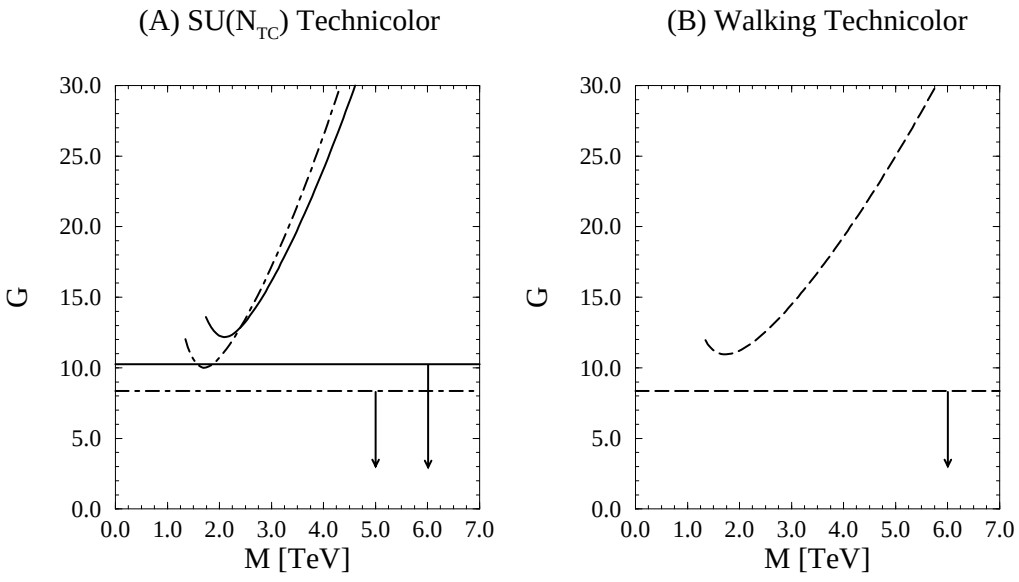
(A) SU(N_TC) Technicolor
(B) Walking Technicolor
G
M [TeV]
30.0
25.0
20.0
15.0
10.0
5.0
0.0
0.0 1.0 2.0 3.0 4.0 5.0 6.0 7.0

Fig. 3

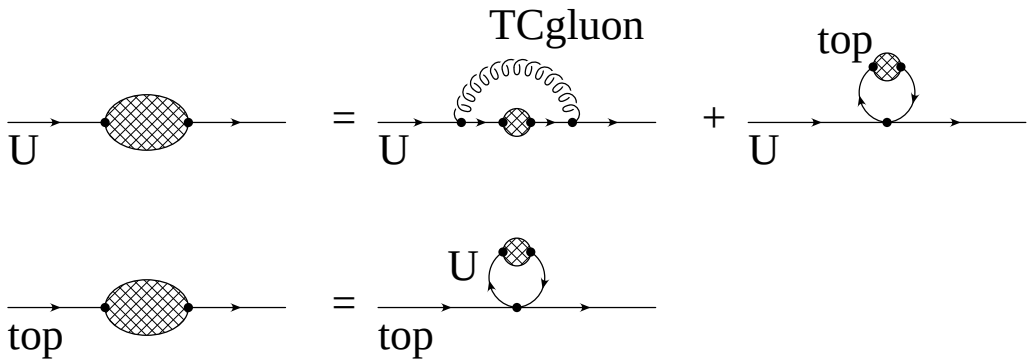

Fig. 4

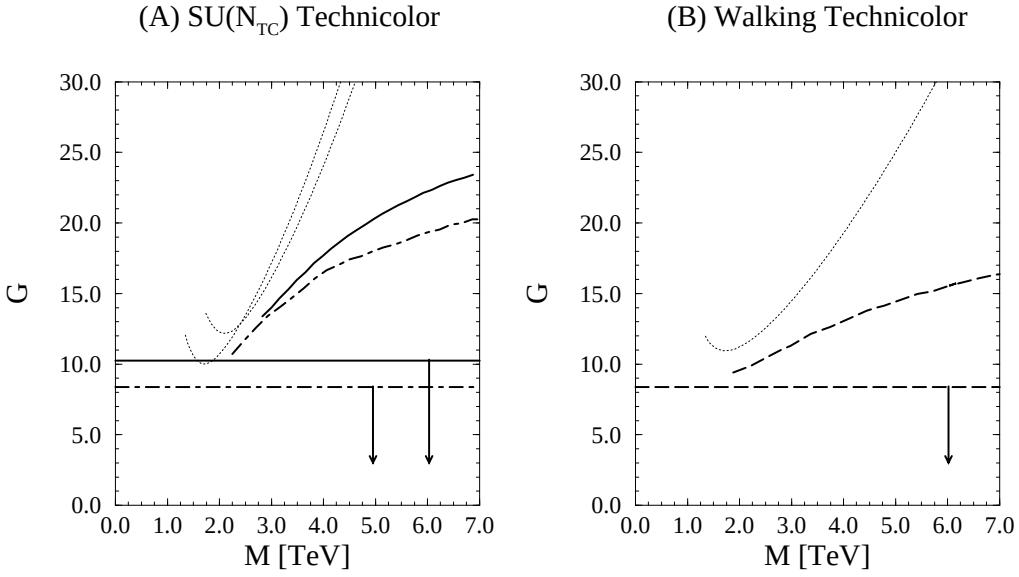
(A) SU(N_TC) Technicolor
(B) Walking Technicolor
G
M [TeV]
30.0
25.0
20.0
15.0
10.0
5.0
0.0
0.0 1.0 2.0 3.0 4.0 5.0 6.0 7.0

Fig. 5

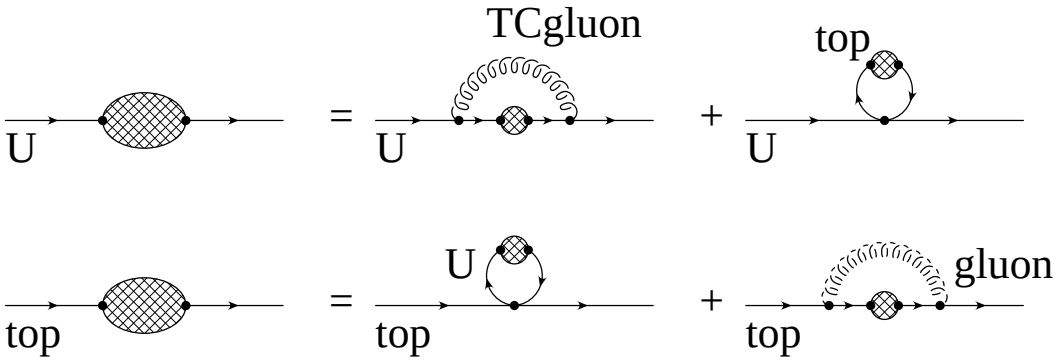

Fig. 6

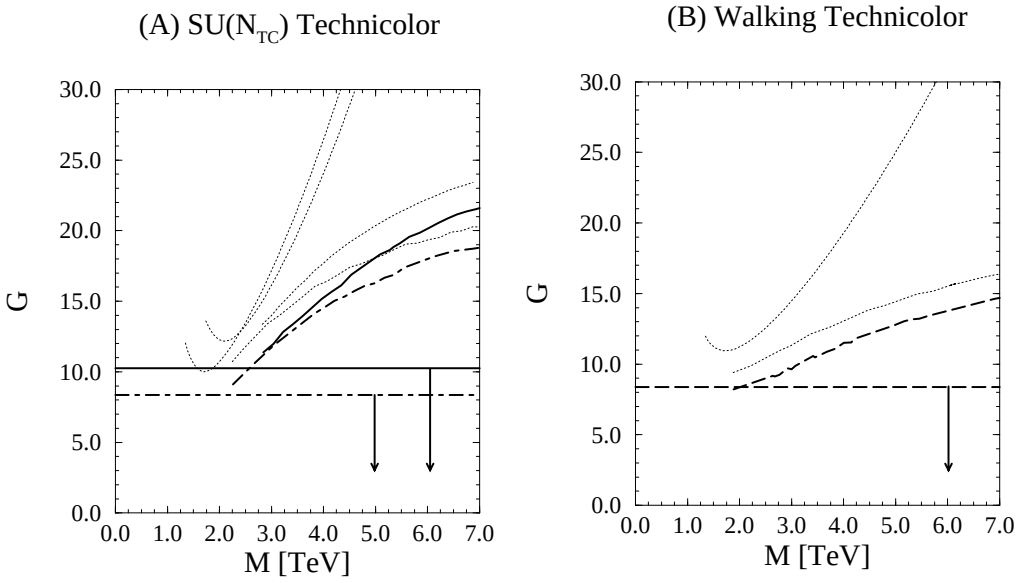
(A) SU(N_TC) Technicolor
(B) Walking Technicolor
G
M [TeV]
30.0
25.0
20.0
15.0
10.0
5.0
0.0
0.0 1.0 2.0 3.0 4.0 5.0 6.0 7.0

Fig. 7

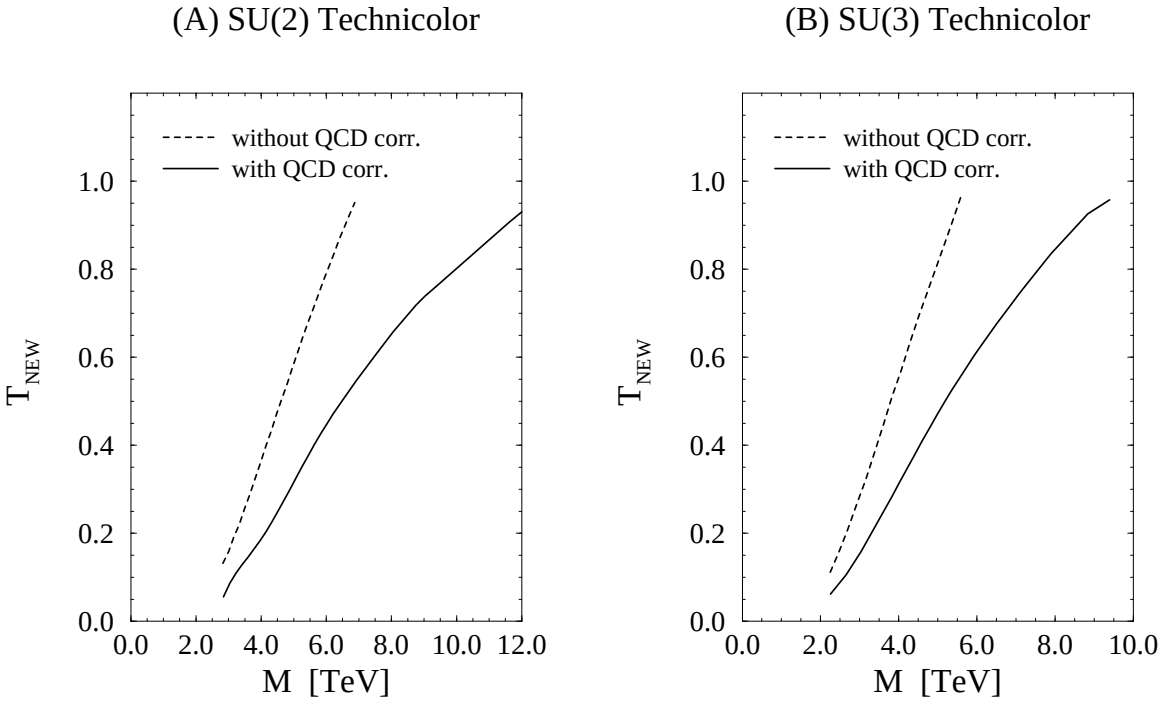
(A) SU(2) Technicolor
(B) SU(3) Technicolor
without QCD corr.
with QCD corr.
T_NEW
M [TeV]
0.0
0.2
0.4
0.6
0.8
1.0
0.0 2.0 4.0 6.0 8.0 10.0 12.0
0.0 2.0 4.0 6.0 8.0 10.0

Fig. 8-(A) and 8-(B)

(C) Walking Technicolor

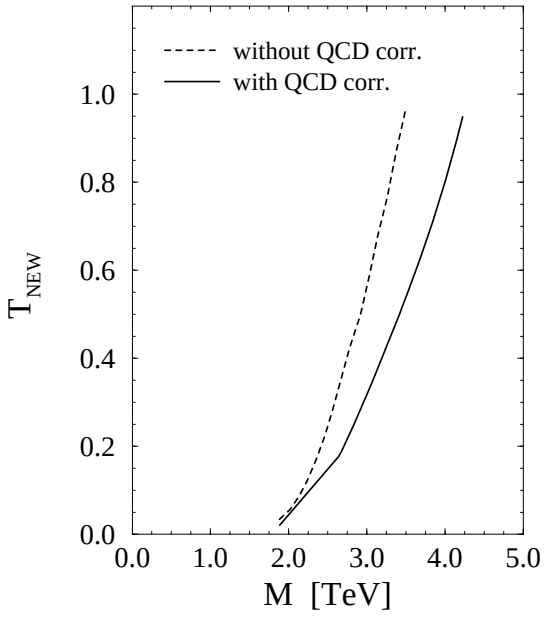

Fig. 8-(C)

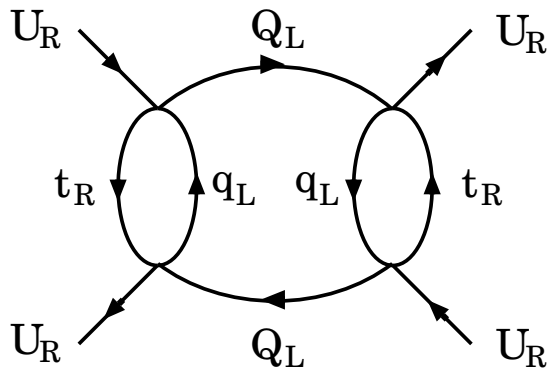

Fig. 9

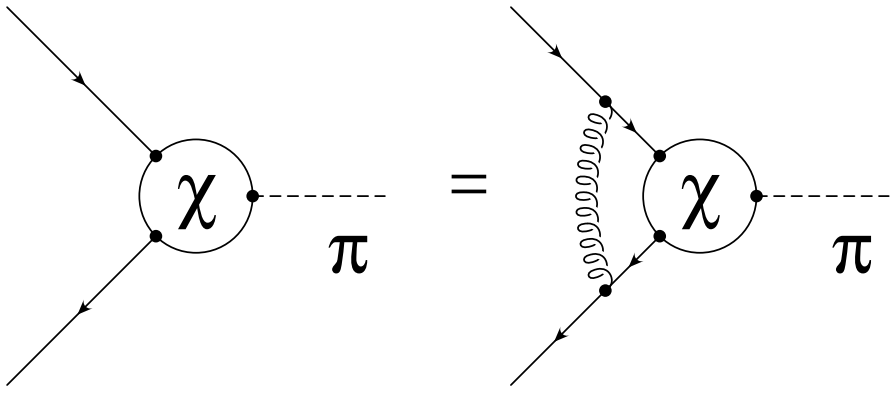

Fig. 10